A HYBRID FINITE-VOLUME-ROM APPROACH TO NON-LINEAR AEROSPACE FLUID-STRUCTURE INTERACTION MODELLING

Andrew G. B. Mowat[1], Arnaud G. Malan[2], Louw H. van Zyl[2], and Josua P. Meyer[3]

[1]Department of Mechanical and Aeronautical Engineering, University of Pretoria
Private bag X20 Hatfield, Pretoria 0028, South Africa
amowat@csir.co.za

[2]Defence Peace Safety and Security, Council for Scientific and Industrial Research
PO Box 395, Pretoria 0001, South Africa
amalan@csir.co.za
lvzyl@csir.co.za

[3]Department of Mechanical and Aeronautical Engineering, University of Pretoria
Private bag X20 Hatfield, Pretoria 0028, South Africa
josua.meyer@up.ac.za

Keywords: ALE, finite volume, FSI, ROMs, transonic, non-linear structure.

Abstract: A fully-coupled partitioned fluid-structure interaction (FSI) scheme is developed for sub- and transonic aeroelastic structures undergoing non-linear displacements. The Euler equations, written in an Arbitrary Lagrangian Eulerian (ALE) coordinate frame, describe the fluid domain while the structure is represented by a quadratic modal reduced order model (ROM). A Runge-Kutta dual-timestepping method is employed for the fluid solver, and three upwind schemes are considered viz. AUSM$^+$ -up, HLLC and Roe schemes. The HLLC implementation is found to offer the superior balance between efficiency and robustness. The developed FSI technology is applied to modelling non-linear flutter, and the quadratic ROM demonstrated to offer dramatic improvements in accuracy over the more conventional linear method.

1 INTRODUCTION

Present day aeroelastic modelling is mature with regards to linear flutter phenomena at subsonic flow speeds [1]. There is still, though, progress required to effect efficient FSI modelling in the transonic flow regime, particularly where a combination of shocks in the fluid domain and non-linear structural response are present. This has led to the growing research into non-linear Computational Aeroelastics [2–15].

Non-linear weakly coupled aeroelastic calculations, such as staggered timestepping methods, may be prone to inaccurate or divergent solutions [16–19]. As a result we employ a strongly coupled partitioned method where coupling is effected via non-linear iterations [19–22]. The fluid domain is resolved by using detailed Computational Fluid Dynamic (CFD) and the structure domain via a non-linear ROM.

To account for the transonic shocks, the fluid is described via the compressible Euler equations written in an ALE reference frame [23–27]. We use a vertex-centred edge-based finite volume method for spacial discretisation and three upwind schemes are compared

viz. AUSM$^+$ -up scheme [28], HLLC scheme [29] and Roe scheme [30]. The MUSCL scheme [31] with van Albada limiter [32] is employed throughout. A fourth order Runge-Kutta dual-time-stepping parallel solution method is employed.

The structure is represented via a quadratic modal ROM [33–35]. This is of particular interest due to its ability to describe non-linear motion from linear modal data. It is also readily applicable to three-dimensional systems. The fluid and solid domains are strongly coupled numerically, where information is passed between the detailed CFD and structural ROM at each sub-iteration.

The developed FSI technology is implemented into the multi-physics code Elemental followed by a verification and validation exercise. The ALE capability is first assessed via modelling of the forced oscillation of a NACA0012 airfoil under transonic flow. The three upwinding schemes are compared via a grid convergence study. Next, the two-dimensional flutter-response of a pitch/plunge airfoil is considered at sub- to transonic flow speeds. We assess the improvement in accuracy of the quadratic modal ROM over the traditional linear modal ROM by comparison to an analytical ROM.

2 GOVERNING EQUATIONS

2.1 Fluid Equations

The fluid dynamics is described via non-dimensional inviscid Euler equations written in an ALE coordinate frame as:

$$\frac{\partial}{\partial t}\int_{\mathcal{V}(t)} \mathbf{U} d\mathcal{V} + \int_{\mathcal{S}(t)} \mathbf{F}^j n_j d\mathcal{S} = 0 \tag{1}$$

where $\mathcal{V}(t)$ denotes an arbitrary moving volume, with surface $\mathcal{S}(t)$ and outward pointing normal vector $\mathbf{n}$, which is translating at velocity $\mathbf{v}$ and

$$\mathbf{U} = \begin{pmatrix} \rho u_1 \\ \rho u_2 \\ \rho \\ \rho E \end{pmatrix} \quad , \quad \mathbf{F}^j = \begin{pmatrix} w_j \rho u_1 + p\delta_{1j} \\ w_j \rho u_2 + p\delta_{2j} \\ w_j \rho \\ w_j \rho E + p u_j \end{pmatrix} \tag{2}$$

In the above equation set, x_j is a fixed Eulerian cartesian reference frame axis, $w_j = u_j - v_j$ is the velocity relative to the moving reference frame, u_j is the fluid velocity, ρ is the density, p is the pressure and E is the specific total energy of the fluid as:

$$E = \frac{p}{(\gamma - 1)\,\rho} + \frac{u_j u_j}{2} \tag{3}$$

Non-dimensional quantities are related to their dimensional counterparts (denoted by $*$) as:

$$\begin{array}{ccccc} t = \frac{t^* U^*_\infty}{L^*} & & x_i = \frac{x_i^*}{L^*} & & u_i = \frac{u_i^*}{U^*_\infty} \qquad \rho = \frac{\rho^*}{\rho^*_\infty} \\ p = \frac{p^*}{(\rho^*_\infty U^{*2}_\infty)} & & T = \frac{T^*}{(U^{*2}_\infty / C_p)} & & E = \frac{E^*}{U^{*2}_\infty} \end{array} \tag{4}$$

where ∞ denotes free-stream, t is time, L is the characteristic length, T is the characteristic temperature and C_p denotes the specific heat at constant pressure.

The governing equations are closed via the ideal gas law as:

$$\rho = \frac{p}{T}\frac{\gamma}{\gamma - 1} \tag{5}$$

while the non-dimensional acoustic velocity is given by

$$c = \sqrt{\frac{\gamma p}{\rho}} \tag{6}$$

which results in $c = c^*/U^*_\infty$.

In order to obtain a unique solution to the ALE Euler equations, appropriate boundary conditions must be specified. For the purpose of this work slip conditions are prescribed on the airfoil surface as:

$$\mathbf{u} \cdot \mathbf{n} = \mathbf{v} \cdot \mathbf{n} \tag{7}$$

where $\mathbf{n}$ and denotes the boundary outward pointing normal unit vector. Characteristic boundary conditions [36] are applied at outer boundaries.

2.2 Solid Equations

For the purpose of this work the aeroelastic structural model is governed by a two degree-of-freedom pitch and plunge system. The equations of motion are

$$\begin{aligned} m\ddot{h} + S_\alpha \ddot{\alpha} + K_h h &= -L \\ S_\alpha \ddot{h} + I_\alpha \ddot{\alpha} + K_\alpha \alpha &= M_{ea} \end{aligned} \tag{8}$$

where

m :	mass of the airfoil per unit span
S_α :	static imbalance
I_α :	sectional moment of inertia of the airfoil
K_h :	plunging spring coefficient
K_α	pitching spring coefficient
h :	vertical displacement (positive down)
α :	angle-of-attack
L :	sectional lift per unit span
M_{ea} :	sectional moment about the elastic centre (positive nose up).

and $\ddot{}$ quantities relate to second-derivatives with respect to time.

3 FLUID DISCRETISATION AND SOLUTION PROCEDURE

3.1 Spacial Discretisation

We discretise the fluid domain via a vertex-centred edge-based finite volume algorithm [37, 38]. It was selected as the method allows natural generic mesh applicability, second-order accuracy without odd-even decoupling, and computational efficiency which is greater than element based approaches.

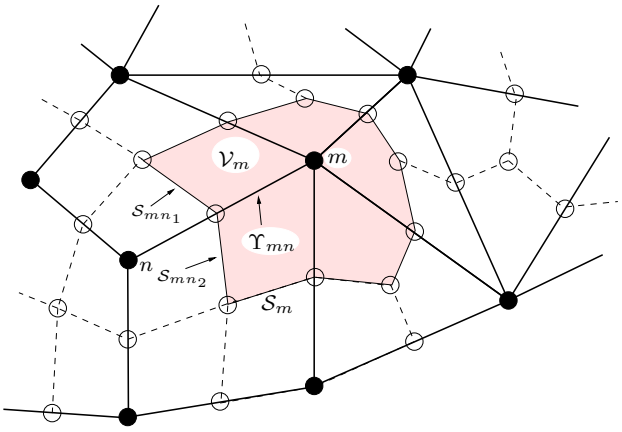

Figure 1: Schematic diagram of the construction of the median dual-mesh on hybrid grids. Here, Υ_{mn} depicts the edge connecting nodes m and n.

The discrete form of the surface integral in Equation (1), computed for the volume $\mathcal{V}_m(t)$ surrounding the node m, is written as:

$$\int_{\mathcal{S}_m(t)} \mathbf{F}^j n_j d\mathcal{S} \approx \sum_{\Upsilon_{mn} \cap \mathcal{V}_m(t)} \overline{\mathbf{F}^j}_{mn} C^j_{mn} \tag{9}$$

where $\overline{\bullet}_{mn}$ quantities denote edge-face values and the volume bounding surface is represented in a discrete manner via edge coefficient $\mathbf{C}_{mn}$. The latter for a given internal edge Υ_{mn} connecting nodes m and n, is defined as a function of time as

$$\mathbf{C}_{mn}(t) = \mathbf{n}^{mn_1} \mathcal{S}_{mn_1}(t) + \mathbf{n}^{mn_2} \mathcal{S}_{mn_2}(t) = \mathbf{n}^{mn} \mathcal{S}_{mn}(t) \tag{10}$$

where $\mathcal{S}_{mn_1}$ is a bounding surface-segment intersecting the edge (Figure 1) and the normal unit vectors are similarly a function of time. For the purpose of calculating the edge-face values, 3 schemes are considered and compared viz. AUSM$^+$ –up, HLLC and Roe schemes. In all cases, 2^{nd} order MUSCL with van Albada limiter [32] is employed.

3.1.1 Roe Scheme

The ALE Roe flux is defined as [39, 40]:

$$\overline{\mathbf{F}^j}_{mn} = \tfrac{1}{2}\left[\mathbf{F}^j(\mathbf{U}_m) + \mathbf{F}^j(\mathbf{U}_n)\right] - \tfrac{1}{2}\sum_{i=1}^{4} |\hat{\lambda}^j_i| \hat{\alpha}^j_i \hat{\mathbf{K}}^j_i \tag{11}$$

where $\hat{}$ are the Roe averaged values, $\hat{\mathbf{K}}$ is the eigenvector and $\hat{\lambda}$ is the eigenvalues of the Jacobian matrix respectively. The wave speed is denoted by $\hat{\alpha}$.

3.1.2 HLLC Scheme

The HLLC flux [41] is calculated as:

$$\overline{\mathbf{F}^j}_{mn} = \begin{cases} \mathbf{F}^j_m & \forall \quad S_m > 0 \\ \mathbf{F}^j(\mathbf{U}^*_m) & \forall \quad S_m \leq 0 < S^* \\ \mathbf{F}^j(\mathbf{U}^*_n) & \forall \quad S^* \leq 0 \leq S_n \\ \mathbf{F}^j_n & \forall \quad S_n < 0 \end{cases} \tag{12}$$

where

$$\mathbf{F}^j(\mathbf{U}^*) = \begin{pmatrix} S^*(\rho u_1)^* + p^* \delta_{1j} \\ S^*(\rho u_2)^* + p^* \delta_{2j} \\ S^* \rho^* \\ S^*(\rho E)^* + (S^* + v_j) p^*] \end{pmatrix} \tag{13}$$

and the * quantities are related to the middle wave speed.

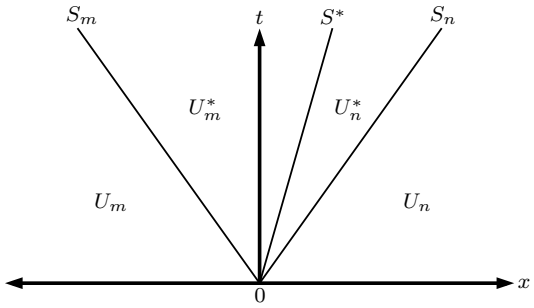

Figure 2: Diagram showing the HLLC Riemann Solver and how the wave speeds S_m, S^* and S_n separate the different regions.

The wave speed S^*, S_m and S_n as shown in Figure 2 are defined as

$$S^* = \frac{\rho_n w_n (S_n - w_n) - \rho_m w_m (S_m - w_m) + p_m - p_n}{\rho_n (S_n - w_n) - \rho_m (S_m - w_m)} \tag{14}$$

and

$$S_m = \min[w_m - c_m, (\hat{\mathbf{u}} - \mathbf{v}) \cdot \mathbf{n} - \hat{c}]; \quad S_n = \max[w_n + c_n, (\hat{\mathbf{u}} - \mathbf{v}) \cdot \mathbf{n} + \hat{c}] \tag{15}$$

where $\hat{\mathbf{u}}$ and $\hat{c}$ are the Roe averages for the velocity vector and the acoustic velocity respectively, which are a function of the left and right nodes.

3.1.3 AUSM$^+$ -up Scheme

The numerical flux of the AUSM$^+$ -up scheme [28] between nodes n and m is defined as follows:

$$\overline{\mathbf{F}^j}_{mn} = \dot{m}_{mn}\vec{\psi}_{mn} + \mathbf{p}_{mn_j} \tag{16}$$

where

$$\vec{\psi}_{mn} = \begin{cases} \vec{\psi}_m & \text{if } \dot{m}_{mn} > 0 \\ \vec{\psi}_n & \text{otherwise} \end{cases} \quad ; \qquad \mathbf{p}_{mn} = \begin{pmatrix} p\delta_{1j} \\ p\delta_{1j} \\ 0 \\ pv_j \end{pmatrix}_{mn} \quad ; \qquad \vec{\psi} = \begin{pmatrix} u_1 \\ u_2 \\ 1 \\ H \end{pmatrix} \tag{17}$$

and $H = E + p/\rho$. Further the mass flux is defined as:

$$\dot{m}_{mn} = c_{mn}M_{mn} \begin{cases} \rho_m & \text{if } M_{mn} > 0 \\ \rho_n & \text{otherwise} \end{cases} \tag{18}$$

where c_{mn} is the acoustic velocity at the interface and the Mach number at the interface is given by

$$M_{mn} = \mathcal{M}^+(M_m) + \mathcal{M}^-(M_n) - K_p \max(1 - \sigma\overline{M}^2, 0)\frac{p_n - p_m}{0.5(\rho_m + \rho_n)c_{mn}^2} \tag{19}$$

where M is the reference Mach number and $\mathcal{M}$ is the Mach number split function. The pressure flux can be written as:

$$p_{mn} = \mathcal{P}^+(M_m)p_m + \mathcal{P}^-(M_n)p_n - K_u\mathcal{P}^+(M_m)\mathcal{P}^-(M_n)(\rho_m + \rho_n)c_{mn}(w_n - w_m) \tag{20}$$

where $\mathcal{P}^+$ and $\mathcal{P}^-$ are the pressure split function.

In the above equations $0 \leq K_p \leq 1$, $\sigma \leq 1$ and $0 \leq K_u \leq 1$, for all the calculations in this work we set $K_p = 0.25$, $\sigma = 1$ and $K_u = 0.75$.

3.2 Temporal Discretisation and Solution Procedure

Consider the following semi-discrete form for the fluid governing equation

$$\frac{d\mathbf{U}}{dt} = -\int_{\mathcal{S}(t)} \mathbf{F}^j n_j dS \tag{21}$$

A dual-time-stepping procedure is employed for solution purposes as

$$\frac{\Delta\mathbf{U}}{\Delta t_\tau}V^\tau = -\int_{\mathcal{S}(t)} \mathbf{F}^j n_j dS\Big|^\tau + \mathbf{S}^\tau V^\tau = \mathbf{R}(\mathbf{U}^{n+1}) \tag{22}$$

where the τ superscript denotes the previous (existing) solution or pseudo time-step and $\Delta t_\tau = t^{\tau+1} - t^\tau$. The source $\mathbf{S}$ is the real-time temporal term which is discretised via a second order backward difference method and fourth-order Runge-Kutta is employed for solution purposes.

4 STRUCTURAL REDUCED ORDER MODEL

The aeroelastic governing Equation (8) may be cast into a non-dimensional ROM form in a manner suitable for solution as

$$\dot{\mathbf{r}} = [\Psi]\,\mathbf{r} + \{\Phi\} \tag{23}$$

where the state vector $\mathbf{r} = \{\mathbf{r}_1, \mathbf{r}_2\}$, with $\mathbf{r}_1 = \{h/b, \alpha\}$ and $\mathbf{r}_2 = \dot{\mathbf{r}}_1$. Here b is the airfoil semi-chord. Further

$$\Psi = \begin{bmatrix} 0 & [\mathbf{I}] \\ -[\mathbf{M}]^{-1}[\mathbf{K}] & 0 \end{bmatrix}; \quad \Phi = \begin{Bmatrix} 0 \\ [\mathbf{M}]^{-1}[\mathbf{Q}] \end{Bmatrix} \tag{24}$$

where $\mathbf{M}$, $\mathbf{K}$ and $\mathbf{I}$ respectively denote the modal mass, stiffness and identity matrices given as

$$\mathbf{M} = \begin{bmatrix} 1 & x_\alpha \\ x_\alpha & r_\alpha^2 \end{bmatrix}; \quad \mathbf{K} = \begin{bmatrix} \left(\frac{\omega_h}{\omega_\alpha}\right)^2 & 0 \\ 0 & r_\alpha^2 \end{bmatrix} \tag{25}$$

where x_α and r_α^2 denote structural parameters defined as $\frac{S_\alpha}{mb}$ and $\frac{I_\alpha}{mb^2}$ respectively. Further, ω_h and ω_α denote the uncoupled natural frequencies of plunge and pitch respectively. The generalised force vector, $\mathbf{Q}$, is calculated for the general case as

$$Q_i = \sum_j^{nodes} \mathbf{f}^j \cdot \frac{d\mathbf{x}^j}{dr_{1_i}} \tag{26}$$

where $\mathbf{x}^j$ and $\mathbf{f}^j$ respectively denote displaced coordinate and aerodynamic force at node j on the airfoil surface. The manner in which x is related to the state vector $\mathbf{r}$ determines the type of ROM which results. In the 2D pitch-plunge case the following analytical expression may be employed

$$\begin{bmatrix} x_1 \\ x_2 \end{bmatrix} = \begin{Bmatrix} \cos\alpha & -\sin\alpha \\ \sin\alpha & \cos\alpha \end{Bmatrix} \begin{bmatrix} x_1^0 - x_1^c \\ x_2^0 - x_2^c \end{bmatrix} + \begin{bmatrix} x_1^c \\ x_2^c - h \end{bmatrix} \tag{27}$$

where x_i^0 is the position at rest ($\alpha = 0$) and x_i^c is the coordinate of the airfoil elastic axis at rest. When considering extension to 3D, an analytical expression is typically not known for the general case, and the norm is to employ an expression which is derived from linear modal analysis viz.

$$\mathbf{x}^j = \mathbf{x}^{0^j} + \sum_i^{modes} r_i \hat{\mathbf{u}}_i^j \tag{28}$$

where $\hat{\mathbf{u}}$ is a normalised linear mode shape (eigen vector), which for the 2D pitch-plunge case is $\hat{\mathbf{u}}_1 = (0, -b)$ and $\hat{\mathbf{u}}_2 = (x_2 - x_2^c, x_1^c - x_1)$. This results in the following generically applicable linear expression for the generalised force vector:

$$Q_i = \sum_{j}^{nodes} \mathbf{f}^j \cdot \hat{\mathbf{u}}_i^j \tag{29}$$

In this work however, we propose to improve on the accuracy of the linear ROM via the use of a so-called *quadratic* extension viz.

$$\mathbf{x}^j = \mathbf{x}^{0^j} + \sum_{i}^{modes} r_i \hat{\mathbf{u}}_i^j + \sum_{i}^{modes} \sum_{k}^{modes} r_i r_k \hat{\mathbf{g}}_{ik}^j \tag{30}$$

which results in no significant additional FSI computational cost. The resulting generalised force expression reads

$$Q_i = \sum_{j}^{nodes} \mathbf{f}^j \cdot \hat{\mathbf{u}}_i^j + \sum_{j}^{nodes} \sum_{k}^{modes} 2 r_k \mathbf{f}^j \cdot \hat{\mathbf{g}}_{ik}^j \tag{31}$$

where for the 2D pitch-plunge case

$$\hat{\mathbf{g}}_{11} = (0,\ 0)\,;\quad \hat{\mathbf{g}}_{12} = (0,\ 0)\,;\quad \hat{\mathbf{g}}_{21} = (0,\ 0)\,;\quad \hat{\mathbf{g}}_{22} = \left(\tfrac{x_{1c}-x_1}{2},\ \tfrac{x_{2c}-x_2}{2}\right) \tag{32}$$

The above results in an initial value problem, for which the spatial accuracy depends on whether the analytical, linear or quadratic expressions are employed. In this work we solve each resulting system accurately via a fourth order Runge-Kutta method, where fourth order Lagrange polynomials are employed to calculate $\mathbf{Q}$ at the second and third steps.

5 FSI SOLUTION AND DYNAMIC MESH MOVEMENT

At the fluid-solid interface, the following equations for traction, displacement and velocity are prescribed:

$$\begin{aligned} (p_f)\, n_j &= -\,(p_s)\, n_j \\ \mathbf{u}_f &= \mathbf{v}_s \\ \mathbf{x}_f &= \mathbf{x}_s \end{aligned} \tag{33}$$

where the subscripts f and s respectively denote fluid and solid and n_j is the related outward pointing normal unit vector. The above are prescribed as part of the pseudo-stepping iterative procedure.

For the purpose of mesh movement, we employ a simple and efficient interpolation scheme which is well suited to parallel computing. Here, an internal node is moved as a function of the displacement of the closest two boundary points (identified at the start of the simulation) as follows:

$$\delta \mathbf{x} = r\delta \mathbf{x}_1 + (1-r)\delta \mathbf{x}_2$$

where $\delta \mathbf{x}_1$ and $\delta \mathbf{x}_2$ are respectively the displacements of the closest internal and external boundary points, and r, which varies between zero and one, is computed as

$$r = \frac{D_2^p}{D_1^p + D_2^p} \text{ with } p = 3/2$$

Here D_1 and D_2 are the distances to the identified boundary points. Since the closest points and the values of r are calculated only once at the beginning of the analysis, the application of the mesh movement function is essentially instantaneous, and the mesh does not deteriorate due to repeated oscillations.

6 EVALUATION

6.1 Transonic Forced Oscillation

Prior to applying the developed technology to an FSI problem, we evaluate its efficiency to predict time-dependent loads. The benchmark problem selected for this purpose is the AGARD test case No. 5 [42], which involves a NACA0012 undergoing forced sinusoidal pitching in flow at a Mach number of $M_\infty = 0.755$. The angle of attack of the airfoil is varied as a function of non-dimensional time t as

$$\alpha = \alpha_0 + \alpha_{max} sin(2k_c t) \tag{34}$$

where $k_c = 0.0814$ denotes the reduced frequency, and the mean and maximum angles of attack are respectively $\alpha_0 = 0.016^\circ$ and $\alpha_{\max} = 2.51^\circ$.

The three upwinding schemes were evaluated via a grid convergence study. For this purpose three unstructured meshes were employed consisting of 5,000; 15,000 and 40,000 vertexes (sample mesh shown in Figure 3). The predicted time varying lift and moment coefficients are depicted in Figures 4. As shown, the calculated unsteady loads compare well with experimental data as well as that of others [23, 24, 26, 43] thus verifying the transonic load calculation aspect of the developed solver.

With regards to scheme comparison, the grid converges indexes (GCIs) [44] for the three upwind schemes on the three meshes are given in Table 1.

Upwind Scheme	GCI
Roe scheme	1.09 %
HLLC scheme	0.93 %
AUSM$^+$ –up scheme	0.38 %

Table 1: Table GCIs for the upwind schemes

The rate of convergence for the three upwind schemes was calculated using the Richardson Extrapolation. Figure 5 shows that the three schemes are between 1^{st} and 2^{nd} order

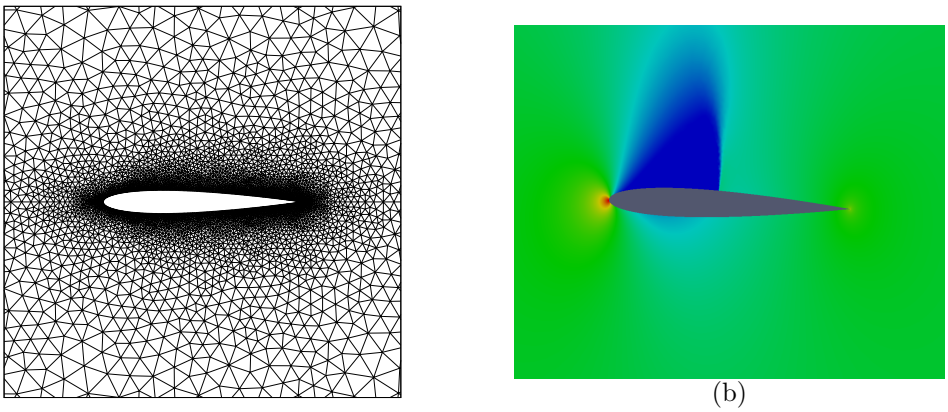

(a) (b)

Figure 3: (a) Mesh employed for the transonic forced oscillation of a NACA0012 airfoil, the mesh consists of 15,000 vertexes. (b) Pressure contours around the NACA0012 airfoil

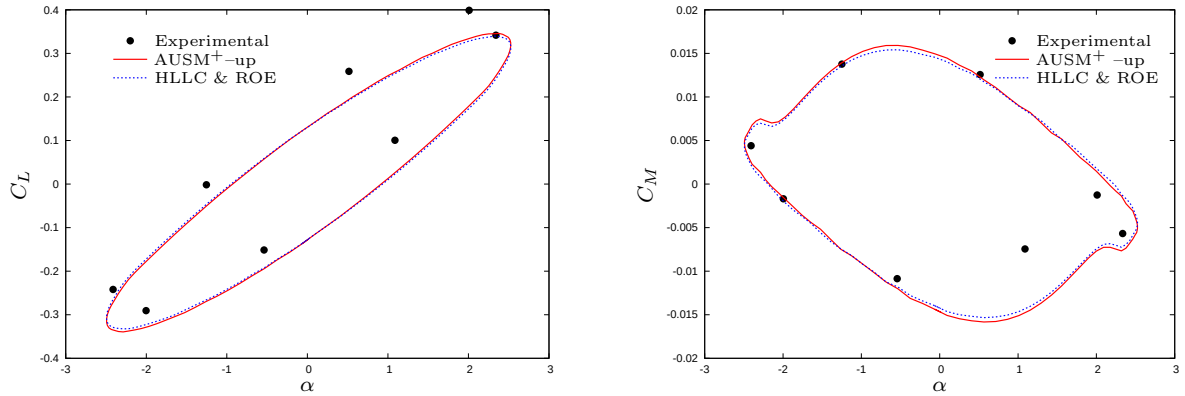

(a) (b)

Figure 4: Graph of (a) C_L versus α and (b) C_M versus α for the forced oscillation of the NACA0012 airfoil

accuracy. This is to be expected as the upwind schemes are reduced to 1^{st} order in the region of the shock. Though AUSM$^+$–up offers superior GCI performance, HLLC shows consistent asymptotic behaviour while being the least costly to compute. As a result, the latter method was employed for the FSI test–cases.

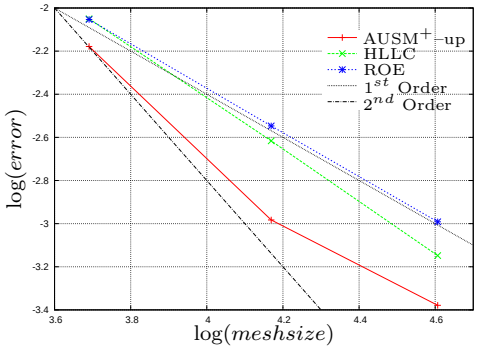

Figure 5: Graph of the difference between the predicted C_L and the Richardson Extrapolation C_L versus mesh size

6.2 Subsonic Flutter

The first FSI test-case consists of the subsonic flutter problem for a NACA64A010 airfoil at $M = 0.3$. The test case is based on the classical incompressible two degree–of–free example of Rodden [45]. In this problem damping has been included into the structural governing equations with the employed structural parameters being

x_α	r_α^2	$\frac{\omega_h}{\omega_\alpha}$	β	a
0.1	0.25	0.4	20	-0.2

where β denotes the airfoil mass ratio and a denotes the non-dimensionalised position along the chord of the elastic centre. The reduced frequency, k_c, corresponds to the linear flutter speed. We use an unstructured mesh consisting of around $5,000$ vortexes. The airfoil is given one forced pitching oscillation where $\alpha_{\max} = 1.0°$ and the mean angle of attack is zero after which it is allowed to interact freely with the fluid. The flutter response calculated via the linear and quadratic ROMs is compared to the analytical method in 6. It is noteworthy that the quadratic ROM offers not only an accurate solution, but a significant improvement over the linear ROM.

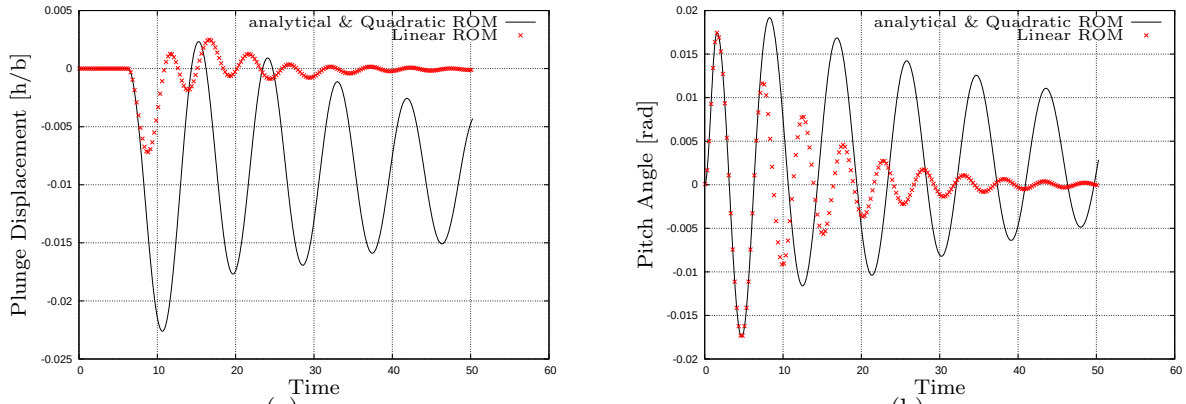

Figure 6: Graph of the (a) Plunge Displacement and the (b) Pitch Angle versus time for the NACA64A010 airfoil, $M_\infty = 0.3$

6.3 Transonic Flutter

The last FSI benchmark problem considers the transonic flow over a two-dimensional representation of a swept-wing (similar to that proposed by Isogai [46]). We however employ the FFAST airfoil (see Acknowledgements), with the following parameters:

x_α	r_α^2	$\frac{\omega_h}{\omega_\alpha}$	β	a
1.8	3.48	1.0	60	-2.0

Here we non-dimensionalise a with the semichord, thus the the elastic centre is positioned half a chord length in front of the leading edge for this problem. The airfoil is given the same forced oscillation as the subsonic case. As previously, the quadratic ROM offers an

accurate solution, while the linear ROM exhibits non-physical decaying amplitudes. The mesh consisting of circa $5,000$ vortexes and is shown in Figure 7.

The results of the analytical, linear ROM and quadratic ROM methods of moving the airfoil are compared in Figure 8. In this problem it is noted that the linear ROM approximation is not as inaccurate as the subsonic case, this is due to smaller rotation of the airfoil.

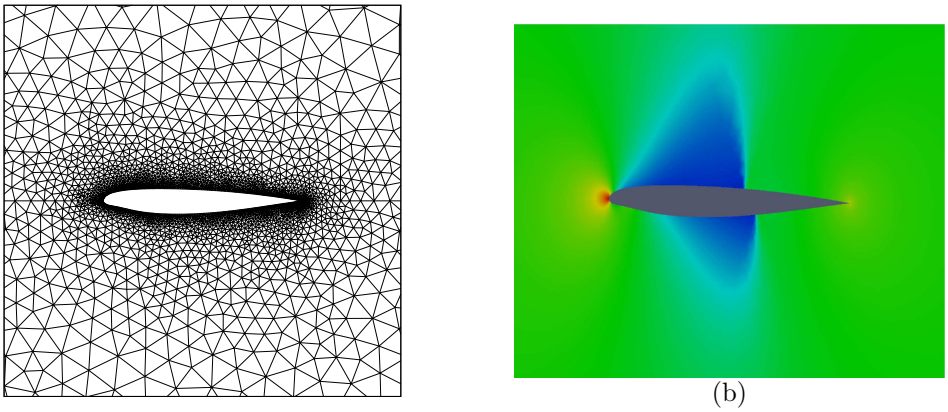

(a) (b)

Figure 7: (a) Mesh employed for the transonic swept-wing model of a FFAST airfoil, the mesh consists of 5000 vertexes. (b) Pressure contours around the FFAST airfoil

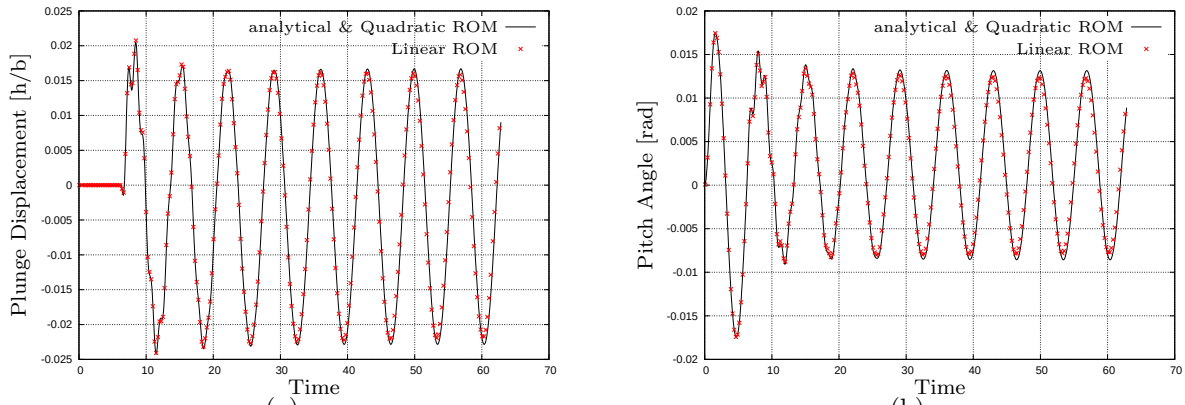

(a) (b)

Figure 8: Graph of the (a) Plunge Displacement and the (b) Pitch Angle versus time for the FFAST airfoil, $M_\infty = 0.8$

7 CONCLUSION

A fully-coupled partitioned FSI scheme was developed for sub- and transonic aeroelastic structures undergoing non-linear displacements. The Euler equations, written in an ALE coordinate frame, described the fluid domain while the structure was represented by a quadratic modal ROM. A Runge-Kutta dual-timestepping method was employed for the fluid solver, and three upwind schemes considered viz. AUSM$^+$ -up, HLLC and Roe schemes. HLLC and AUSM$^+$ -up were shown to be notionally second-order accurate, but the HLLC implementation was found to offer the superior balance between efficiency and robustness. The developed FSI technology was applied to modelling non-linear flutter, and the quadratic modal ROM demonstrated to offer dramatic improvements in accuracy over the more conventional linear modal method.

8 ACKNOWLEDGEMENTS

The research leading to these results has received funding from the European Communitys Seventh Framework Programme (FP7 / 2007-2013) under a grant agreement number 233665. FFAST (Future Fast Aeroelastic Simulation Technologies) is a collaborative research project aimed at developing, implementing and assessing a range of numerical simulation technologies to accelerate future aircraft design. Advances in critical load identification and reduced order modelling methods will potentially provide a step change in the efficiency and accuracy of the dynamic aeroelastic loads process. The partners in FFAST are: University of Bristol, INRIA, CSIR, TU Delft, DLR, IRIAS, University of Liverpool, Politecnico di Milano, NUMECA, Optimad Engineering, Airbus, EADS-MS and IITP.

9 REFERENCES

[1] Guruswamy, G. P. (2002). A review of numerical fluids/structures interface methods for computations using high-fidelity equations. *Computers & Structures*, 80(1), 31 – 41.

[2] Strgnac, T. W. and Mook, D. T. (1990). Numerical model of unsteady subsonic aeroelastic behaviour. *AIAA Journal*, 28, 903–909.

[3] Lee-Raush, E. M. and Batina, J. T. (1993). Wing flutter boundary prediction using unsteady euler aerodynamic method. *AIAA Paper*, 93-1422.

[4] C. Farhat, M. L. and Maman, N. (1995). Mixed explicit/implicit time integration of coupled aeroelastic problems: three-field formulation, geometric conservation and distributed solution. *International Journal for Numerical Methods in Fluids*, 21, 807–835.

[5] S. Piperno, C. F. and Larrouturou, B. (1995). Partitioned procedures for the transient solution of coupled aeroelastic problems. *Computer Methods in Applied Mechanics and Engineering*, 124, 11–79.

[6] Bennet, R. M. and Edwards, J. W. (1998). An overview of recent developments in computational aeroelasticity. In *Proceedings of the 29th AIAA fluid dynamics conference, Albuquerque, NM.*

[7] Lesoinne, M. and Farhat, C. (1998). A higher-order subiteration free staggered algorithm for nonlinear transient aeroelastic problems. *AIAA Journal*, 36, 1754–1756.

[8] C. Felippa, K. C. P. and Farhat, C. (2001). Partitioned analysis of coupled mechanical systems. *Computer Methods in Applied Mechanics and Engineering*, 190, 3247–3270.

[9] Piperno, S. and Farhat, C. (2001). Partitioned procedures for the transient solution of coupled aeroelastic problems—Part II: Energy transfer analysis and three-dimensional applications. *Computer Methods in Applied Mechanics and Engineering*, 190, 3147–3170.

[10] C. Farhat, P. G. and Brown, G. (2003). Application of a three-field nonlinear fluid–structure formulation to the prediction of the aeroelastic parameters of an F-16 fighter. *Computers and Fluids*, 32, 3–29.

[11] Kroyer, R. (2003). FSI analysis in supersonic fluid flow. *Computers and Structures*, 81, 755–764.

[12] Yurkovich, R. (2003). Status of unsteady aerodynamic prediction for flutter of high-performance aircraft. *Journal of Aircraft*, 40, 832–842.

[13] Kamakoti, R. (2004). Fluid–structure interaction for aeroelastic applications. *Progress in Aerospace Sciences*, 40, 535–558.

[14] C. Farhat, K. G. v. d. Z. and Geuzaine, P. (2006). Provably second-order time-accurate loosely-coupled solution algorithms for transient nonlinear computational aeroelasticity. *Computer Methods in Applied Mechanics and Engineering*, 195, 1973–2001.

[15] L. Cavagna, G. Q. and Mantegazza, P. (2007). Application of navier–stokes simulations for aeroelastic stability assessment in transonic regime. *Computers and Structures*, 85, 818–832.

[16] Hübner, B., Walhorn, E., and Dinkler, D. (2004). A monolithic approach to fluid–structure interaction using spacetime finite elements. *Comput. Methods Appl. Mech. Engrg.*, 193, 2087–2104.

[17] Greenshields, C. J. and Weller, H. G. (2005). A unified formulation for continuum mechanics applied to fluid-structure interaction in flexible tubes. *Int. J. Numer. Meth. Engng*, 64, 1575–1593.

[18] Dettmer, W. and Peric, J. D. (2006). A computational framework for fluid–structure interaction: Finite element formulation and application. *Comput. Meth. Appl. Mech. Engrng.*, 195, 5754–79.

[19] Wall, W. A., Genkinger, S., and Ramm, E. (2007). A strong coupling partitioned approach for fluid–structure interaction with free surfaces. *Computers & Fluids*, 36, 169–183.

[20] Tallec, P. L. and Mouro, J. (2001). Fluid structure interaction with large structural displacements. *Computer Methods in Applied Mechanics and Engineering*, 190, 3039–3067.

[21] Matthies, H. G. and Steindorf, J. (2002). Partitioned but strongly coupled iteration schemes for nonlinear fluid–structure interaction. *Computers and Structures*, 80, 1991–1999.

[22] Matthies, H. G. and Steindorf, J. (2003). Partitioned strong coupling algorithms for fluid–structure interaction. *Computers and Structures*, 81, 805–812.

[23] Alonso, J. J. and Jameson, A. (1994). Fully implicit time-marching aeroelastic solutions. In *32nd AIAA Aerospace Sciences Meeting and Exhibit*, vol. AIAA Paper 94-0056. Reno, NV.

[24] Willcox, K. and Peraire, J. (1997). Aeroelastic computations in the time domian using unstructured meshes. *International Journal for Numerical methods in Engineering*, 40, 2413–2431.

[25] H. Luo, J. D. B. and Löhner, R. (2004). On the computation of multi-material flows using ale formulation. *Journal of Computational Physics*, 194(1), 304–328.

[26] Mani, K. and Mavriplis, D. J. (2008). Linearization of the coupled unsteady fluid-structure equations: Application to flutter control. In *AIAA*, vol. Paper 2008-6242. Honolulu.

[27] Schieffer, G., Ray, S., Bramkamp, F. D., et al. (2010). *An Adaptive Implicit Finite Volume Scheme for Compressible Turbulent Flows about Elastic Configurations*, vol. 109. Springer Berlin / Heidelberg.

[28] Liou, M. S. (2006). A sequel to AUSM, part II: AUSM$^+$ -up for all speeds. *Journal of Computational Physics*, 214, 137 – 170.

[29] E. F. Toro, M. S. and Speares, W. (1994). Restoration of the contact surface in the hll-riemann solver. *Shock Waves*, 4, 25–34.

[30] Roe, P. L. (1981). Approximate riemann solvers, parameter vectors, and difference schemes. *Journal of Computational Physics*, 43(2), 357–372.

[31] van Leer, B. (1979). Toward the ultimate conservative scheme v: A second order sequel to godunov's method. *Journal of Computational Physics*, 32, 101–136.

[32] van Albada, G. D., van Leer, B., and Roberts, W. W. (1982). A comparative study of computational methods in cosmic gas dynamics. *Astronomy and Astrophysics*, 108(1), 76–84.

[33] Dohrmann, C. R. and Segalman, D. J. (1996). *Use of Quadratic Components for Buckling Calculations*. Albuquerque: Sandia National Laboratories, technical report no. sand-96-2367c ed.

[34] Segalman, D. J. and Dohrmann, C. R. (1996). A method for calculating the dynamics of rotating flexible structures, part 1: Derivation. *Journal of Vibration and Acoustics*, 118, 313–317.

[35] Segalman, D. J., Dohrmann, C. R., and Slavin, A. M. (1996). A method for calculating the dynamics of rotating flexible structures, part 2: Example calculations. *Journal of Vibration and Acoustics*, 118, 318–322.

[36] Thomas, J. L. and Salas, M. D. (1986). Far field boundary conditions for transonic lifting solutions to euler equations. *AIAA Journal*, 24, 1074–1080.

[37] Sørensen, K. A., Hassan, O., Morgan, K., et al. (2002). Agglomerated multigrid on hybrid unstructured meshes for compressible flow. *International Journal for Numerical Methods in Fluids*, 40(3-4), 593–603.

[38] Malan, A. G., Lewis, R. W., and Nithiarasu, P. (2002). An improved unsteady, unstructured, artificial compressibility, finite volume scheme for viscous incompressible flows: Part I. Theory and implementation. *International Journal for Numerical Methods in Engineering*, 54(5), 695–714.

[39] Toro, E. F. (1999). *Riemann Solvers and Numerical Methods for Fluid Dynamics – A Practical Introduction*. Berlin: Springer - Verlag, second ed.

[40] Trépanier, J., Reggio, M., Zhang, H., et al. (1991). A finite-volume method for the euler equations on arbitrary lagrangian-eulerian grids. *Computers & Fluids*, 20(4), 399–409.

[41] P. Batten, M. A. L. and Goldberg, U. C. (1997). Average-state jacobians and implicit methods for compressible viscous and turbulent flows. *Journal of Computational Physics*, 137, 38–78.

[42] AGARD (1982). *Compendium of Unsteady Aerodynamic Measurements*. AGARD Report No. 702.

[43] Batina, J. T. (1990). Unsteady euler airfoil solutions using unstructured dynamic meshes. *AIAA Journal*, 28–8, 1381–1388.

[44] Roache, P. (1998). *Verification and Validation in Computational Science and Engineering*. New Mexico: Hermosa Publishers.

[45] Rodden, W. P. and Bellinger, E. D. (1982). Aerodynamic lag functions, divergence, and the british flutter method. *Journal of Aircraft*, 19(7), 596–598.

[46] Isogai, K. (1981). Transonic dip mechanics of flutter of a sweptback wing: Part ii. *AIAA Journal*, 17, 1240–1242.